Available online at www.sciencedirect.com
ScienceDirect
Journal of Sound and Vibration 317 (2008) 955–974
JOURNAL OF SOUND AND VIBRATION
www.elsevier.com/locate/jsvi

Mesh-free least-squares-based finite difference method for large-amplitude free vibration analysis of arbitrarily shaped thin plates

W.X. Wu[a], C. Shu[a,*], C.M. Wang[b]

[a]Department of Mechanical Engineering, National University of Singapore, 10 Kent Ridge Crescent, Singapore 117576, Singapore
[b]Engineering Science Programme and Department of Civil Engineering, National University of Singapore, 10 Kent Ridge Crescent, Singapore 117576, Singapore

Received 11 May 2007; received in revised form 30 November 2007; accepted 30 March 2008
Handling Editor: L.G. Tham
Available online 16 May 2008

Abstract

A mesh-free least-squares-based finite difference (LSFD) method is applied for solving large-amplitude free vibration problem of arbitrarily shaped thin plates. In this approximate numerical method, the spatial derivatives of a function at a point are expressed as weighted sums of the function values of a group of supporting points. This method can be used to solve strong form of partial differential equations (PDEs), and it is especially useful in solving problems with complex domain geometries due to its mesh-free and local approximation characteristics. In this study, the displacement components of thin plates are constructed from the product of a spatial function and a periodic temporal function. Consequently, the nonlinear PDE is reduced to an ordinary differential equation (ODE) in terms of the temporal function. The accuracy, simplicity and efficiency of this mesh-free method are demonstrated for plates with simple as well as complex shapes. The ODE solutions obtained allow one to investigate the effect of large deflection amplitude on the vibration frequencies or periods.

1. Introduction

When flexural deflection amplitudes are small relative to the plate thickness, the effect of in-plane forces can be neglected and the free vibration problem is governed by a linear fourth-order partial differential equation (PDE) if the classical thin plate theory is adopted. However, when the vibration amplitudes are not small, in-plane stretching (and thus in-plane forces) becomes significant and this effect has to be taken into consideration, otherwise the frequencies will be under-predicted. Therefore, for large-amplitude free vibration of plates, some nonlinear terms that account for the effect of in-plane forces should be included in the governing PDE (see for example, Refs. [1–3]). The resulting nonlinear PDE is much more difficult to solve than the original linear PDE. So far, no exact solution to this nonlinear PDE for any shape of plate has been given in the literature, although some approximate analytical and numerical solutions have been reported.

*Corresponding author. Tel.: +65 68746476; fax: +65 67791459.
E-mail address: mpeshuc@nus.edu.sg (C. Shu).

0022-460X/$ - see front matter
doi:10.1016/j.jsv.2008.03.050

In obtaining these approximate solutions, Chu and Herrmann [4] used a perturbation procedure to solve the nonlinear PDE directly and approximately for the case of rectangular plates with simply supported, immovable edges. Yamaki [5] extended the work of Chu and Herrmann [4] by treating rectangular and circular plates with various boundary conditions. Based on Berger's hypothesis [6], Wah [7] solved a simplified nonlinear PDE in which the in-plane forces are replaced by a single membrane force. He considered rectangular plates with two simply supported edges opposite to each other. Mei [8] also used Berger's hypothesis in his finite element formulation for the large-amplitude free vibration of rectangular plates. In the aforementioned studies, the fundamental nonlinear frequencies were obtained.

More recently, some researchers turned their attention to computing the higher modes of large-amplitude free vibration of plates. Rao et al. [9,10] used a finite element formulation together with the Ritz procedure for determining the nonlinear frequencies of rectangular and circular plates with various boundary conditions. Mei et al. [11] also applied a finite element formulation for analyzing large-amplitude free vibration of plates with different shapes. Wang et al. [12] used a boundary integral equation formulation for square and circular plates with various boundary conditions. Shi and Mei [13] used a finite element time domain modal formulation for tackling square and L-shaped plates. Kurpa et al. [14] used an *R*-function method for some complicated plate shapes. Barik and Mukhopadhyay [15] constructed a new stiffened plate element for the analysis of arbitrarily shaped plates with stiffeners.

In this study, following the work by Chu and Herrmann [4], Wah [7] and Mei [8], the mode shapes of large-amplitude free vibration are assumed to be similar to their linear small-amplitude counterparts. In other words, the effect of in-plane forces on the mode shapes and the effect of vibration mode coupling are neglected. By using the mesh-free LSFD method, the linear frequencies and corresponding mode shapes can be readily obtained for arbitrarily shaped plates. The modal in-plane displacements can be solved from their coupling relations with the mode shapes. The *real* transverse and in-plane displacements of plates are assumed as a product of a spatial function (mode shapes or modal in-plane displacements) and a periodic temporal function. This assumption leads to the reduction of the nonlinear governing PDE into an ordinary differential equation (ODE) in terms of the temporal function. The coefficients associated with the temporal function in the ODE can be calculated from the derived modal transverse deflection and modal in-plane displacements. With the appropriate initial conditions, the temporal function can be easily solved numerically, and the large-amplitude free vibration frequencies or periods determined.

For more information on the use of mesh-free methods that are closely related with the present study in solving structural problems, one may refer to Refs. [16–26].

2. Least-squares-based finite difference (LSFD) method

In this section, the methodology of the LSFD method is briefly described. A detailed description of the method may be obtained from Ding et al. [16]. For an unstructured distribution of points in a computational domain, as shown in Fig. 1, the index i represents a typical point and ij a group of points near the point i (hereafter ij is referred to as the supporting points of the point i). For a continuous and differentiable function $f(x, y)$, the two-dimensional (2D) Taylor series expansion in the Δ-form can be written as

$$\begin{aligned}\Delta f_{ij} &= \Delta x_{ij}\frac{\partial f_i}{\partial x} + \Delta y_{ij}\frac{\partial f_i}{\partial y} + \frac{\Delta x_{ij}^2}{2}\frac{\partial^2 f_i}{\partial x^2} + \frac{\Delta y_{ij}^2}{2}\frac{\partial^2 f_i}{\partial y^2} + \Delta x_{ij}\Delta y_{ij}\frac{\partial^2 f_i}{\partial x \partial y} \\ &\quad + \frac{\Delta x_{ij}^3}{6}\frac{\partial^3 f_i}{\partial x^3} + \frac{\Delta y_{ij}^3}{6}\frac{\partial^3 f_i}{\partial y^3} + \frac{\Delta x_{ij}^2 \Delta y_{ij}}{2}\frac{\partial^3 f_i}{\partial x^2 \partial y} + \frac{\Delta x_{ij}\Delta y_{ij}^2}{2}\frac{\partial^3 f_i}{\partial x \partial y^2} + O(h^4)\end{aligned} \tag{1}$$

where $\Delta f_{ij} = f_{ij} - f_i$, $\Delta x_{ij} = x_{ij} - x_i$, $\Delta y_{ij} = y_{ij} - y_i$; (x_i, y_i) and (x_{ij}, y_{ij}) are the Cartesian coordinates of the points i and ij, respectively; f_i and f_{ij} are the function values at the points i and ij, respectively; $\partial f_i/\partial x$ represents the value of $\partial f/\partial x$ at the point i, and other expressions for derivatives in Eq. (1) have similar meanings; h in $O(h^4)$ is the mean distance from the supporting points ij to the point i.

In LSFD method, the derivatives in Eq. (1) are considered as unknowns. Eq. (1) has nine unknowns, i.e., two first-order derivatives, three second-order derivatives and four third-order derivatives. In order to determine the nine unknowns, we need nine independent equations which can be obtained by applying Eq. (1)

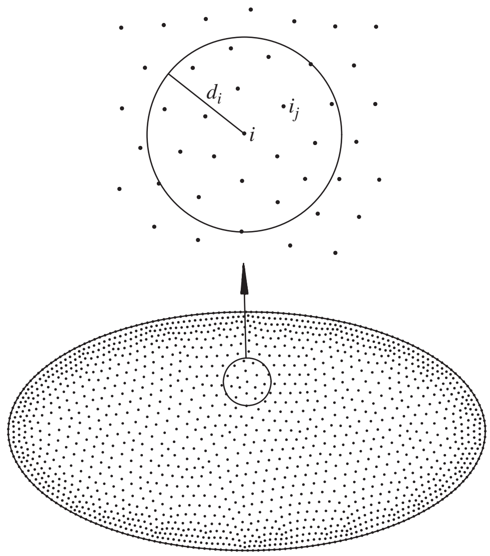

Fig. 1. A computational domain with an unstructured distribution of points.

at nine supporting points and neglecting the truncation errors $O(h^4)$ in Eq. (1). The resulting system of equations may be expressed in a compact form:

$$\Delta \mathbf{f}_i = \mathbf{S}_i \, \mathrm{d}\mathbf{f}_i \tag{2}$$

where

$$\Delta \mathbf{f}_i = \begin{bmatrix} \Delta f_{i1} & \Delta f_{i2} & \cdots & \Delta f_{i9} \end{bmatrix}^{\mathrm{T}} \tag{3}$$

$$\mathrm{d}\mathbf{f}_i = \begin{bmatrix} \dfrac{\partial f_i}{\partial x} & \dfrac{\partial f_i}{\partial y} & \dfrac{\partial^2 f_i}{\partial x^2} & \dfrac{\partial^2 f_i}{\partial y^2} & \dfrac{\partial^2 f_i}{\partial x \partial y} & \dfrac{\partial^3 f_i}{\partial x^3} & \dfrac{\partial^3 f_i}{\partial y^3} & \dfrac{\partial^3 f_i}{\partial x^2 \partial y} & \dfrac{\partial^3 f_i}{\partial x \partial y^2} \end{bmatrix}^{\mathrm{T}} \tag{4}$$

$$\mathbf{S}_i = \begin{bmatrix} \Delta x_{i1} & \Delta y_{i1} & \dfrac{\Delta x_{i1}^2}{2} & \dfrac{\Delta y_{i1}^2}{2} & \Delta x_{i1}\Delta y_{i1} & \dfrac{\Delta x_{i1}^3}{6} & \dfrac{\Delta y_{i1}^3}{6} & \dfrac{\Delta x_{i1}^2 \Delta y_{i1}}{2} & \dfrac{\Delta x_{i1}\Delta y_{i1}^2}{2} \\ \Delta x_{i2} & \Delta y_{i2} & \dfrac{\Delta x_{i2}^2}{2} & \dfrac{\Delta y_{i2}^2}{2} & \Delta x_{i2}\Delta y_{i2} & \dfrac{\Delta x_{i2}^3}{6} & \dfrac{\Delta y_{i2}^3}{6} & \dfrac{\Delta x_{i2}^2 \Delta y_{i2}}{2} & \dfrac{\Delta x_{i2}\Delta y_{i2}^2}{2} \\ \vdots & \vdots & \vdots & \vdots & \vdots & \vdots & \vdots & \vdots & \vdots \\ \Delta x_{i9} & \Delta y_{i9} & \dfrac{\Delta x_{i9}^2}{2} & \dfrac{\Delta y_{i9}^2}{2} & \Delta x_{i9}\Delta y_{i9} & \dfrac{\Delta x_{i9}^3}{6} & \dfrac{\Delta y_{i9}^3}{6} & \dfrac{\Delta x_{i9}^2 \Delta y_{i9}}{2} & \dfrac{\Delta x_{i9}\Delta y_{i9}^2}{2} \end{bmatrix} \tag{5}$$

In the matrix $\mathbf{S}_t$, the entries are the coefficient factors of the derivatives in Eq. (1).

In order to solve Eq. (2), we need to invert the matrix $\mathbf{S}_t$. It has been observed that the matrix $\mathbf{S}_t$ tends to be ill-conditioned numerically when one or more of the supporting points are very close to the reference point i, i.e. $\Delta x_{ij} \approx 0$, $\Delta y_{ij} \approx 0$ for some j. In addition, it was found that the matrix $\mathbf{S}_t$ may become singular when some supporting points are very close to each other. To overcome this difficulty, the radius d_i of the supporting region (see Fig. 1) is used to scale the local distance $(\Delta x_{ij}, \Delta y_{ij})$, i.e.

$$\Delta \bar{x}_{ij} = \frac{\Delta x_{ij}}{d_i}, \quad \Delta \bar{y}_{ij} = \frac{\Delta y_{ij}}{d_i} \tag{6}$$

The local scaling process is equivalent to introducing a diagonal matrix $\mathbf{D}_i$ of the form

$$\mathbf{D}_i = \mathrm{diag}\,(d_i, d_i, d_i^2, d_i^2, d_i^2, d_i^3, d_i^3, d_i^3, d_i^3) \tag{7}$$

In view of Eq. (2), we can write

$$\Delta \mathbf{f}_i = \overline{\mathbf{S}}_i \, \mathrm{d}\overline{\mathbf{f}}_i \tag{8}$$

where

$$\overline{\mathbf{S}}_i = \mathbf{S}_i \mathbf{D}_i^{-1}, \quad \mathrm{d}\overline{\mathbf{f}}_i = \mathbf{D}_i \, \mathrm{d}\mathbf{f}_i \tag{9a,b}$$

By local scaling, the condition number of the matrix $\overline{\mathbf{S}}_i$ becomes lower than the original matrix $\mathbf{S}_i$. On the other hand, the point distribution in the LSFD method could be random. The irregular point distribution may also cause the matrix $\mathbf{S}_i$ to be ill-conditioned or even singular, which cannot be improved by local scaling. In order to overcome this difficulty, we can introduce the weighted least-squares optimization to determine the unknown vector $\mathrm{d}\overline{\mathbf{f}}_i$ in the approximate Eq. (8). This process is described below.

Apply Eq. (1) at m supporting points ij ($j = 1,2,\ldots,m$; $m>9$) for the reference point i so as to approximate the values of Δf_{ij}. The same form of Eqs. (2)–(9) can be obtained by following a procedure that is similar to the one discussed above, except that the vector $\Delta \mathbf{f}_i$ in Eq. (3) and the matrix $\mathbf{S}_i$ in Eq. (5) have to be modified, i.e.,

$$\Delta \mathbf{f}_i = \begin{bmatrix} \Delta f_{i1} & \Delta f_{i2} & \cdots & \Delta f_{im} \end{bmatrix}^{\mathrm{T}} \tag{10}$$

$$\mathbf{S}_i = \begin{bmatrix} \Delta x_{i1} & \Delta y_{i1} & \dfrac{\Delta x_{i1}^2}{2} & \dfrac{\Delta y_{i1}^2}{2} & \Delta x_{i1}\Delta y_{i1} & \dfrac{\Delta x_{i1}^3}{6} & \dfrac{\Delta y_{i1}^3}{6} & \dfrac{\Delta x_{i1}^2 \Delta y_{i1}}{2} & \dfrac{\Delta x_{i1}\Delta y_{i1}^2}{2} \\ \Delta x_{i2} & \Delta y_{i2} & \dfrac{\Delta x_{i2}^2}{2} & \dfrac{\Delta y_{i2}^2}{2} & \Delta x_{i2}\Delta y_{i2} & \dfrac{\Delta x_{i2}^3}{6} & \dfrac{\Delta y_{i2}^3}{6} & \dfrac{\Delta x_{i2}^2 \Delta y_{i2}}{2} & \dfrac{\Delta x_{i2}\Delta y_{i2}^2}{2} \\ \vdots & \vdots & \vdots & \vdots & \vdots & \vdots & \vdots & \vdots & \vdots \\ \Delta x_{im} & \Delta y_{im} & \dfrac{\Delta x_{im}^2}{2} & \dfrac{\Delta y_{im}^2}{2} & \Delta x_{im}\Delta y_{im} & \dfrac{\Delta x_{im}^3}{6} & \dfrac{\Delta y_{im}^3}{6} & \dfrac{\Delta x_{im}^2 \Delta y_{im}}{2} & \dfrac{\Delta x_{im}\Delta y_{im}^2}{2} \end{bmatrix} \tag{11}$$

The unknown vector $\mathrm{d}\overline{\mathbf{f}}_i$ in Eq. (8) will be obtained by minimizing the summation of the weighted squares of the approximation errors of Eq. (8). This summation is given by

$$J_i = \sum_{j=1}^{m} V_{ij} \left[\Delta f_{ij} - \sum_{k=1}^{9} (\overline{\mathbf{S}}_i)_{j,k} \cdot (\mathrm{d}\overline{\mathbf{f}}_i)_k \right]^2 = (\Delta \mathbf{f}_i - \overline{\mathbf{S}}_i \, \mathrm{d}\overline{\mathbf{f}}_i)^{\mathrm{T}} \mathbf{V}_i (\Delta \mathbf{f}_i - \overline{\mathbf{S}}_i \, \mathrm{d}\overline{\mathbf{f}}_i) \tag{12}$$

where

$$\mathbf{V}_i = \mathrm{diag}(V_{i1}, V_{i2}, \ldots, V_{im}) \tag{13}$$

is the weighting function matrix with compact support, i.e., the values of V_{ij} ($j = 1,2,\ldots,m$) are chosen in such a way that the supporting point closer to the reference point i has a greater influence on the function value at the point i. The weighting function that is normally adopted is

$$V_{ij} = \sqrt{4/\pi}(1 - \bar{r}_{ij}^2)^4 \tag{14}$$

where $\bar{r}_{ij} = \sqrt{\Delta x_{ij}^2 + \Delta y_{ij}^2}/d_i \leqslant 1$, and d_i is the radius of supporting region of point i. Other forms of weighting functions may also be used, such as

$$V_{ij} = 1/\bar{r}_{ij} \tag{15a}$$

$$V_{ij} = 1 - 6\bar{r}_{ij}^2 + 8\bar{r}_{ij}^3 - 3\bar{r}_{ij}^4 \tag{15b}$$

$$V_{ij} = 1/\bar{r}_{ij}^4 \tag{15c}$$

In order to find $\mathrm{d}\overline{\mathbf{f}}_i$, we need to minimize J_i by making

$$\frac{\partial J_i}{\partial(\mathrm{d}\overline{\mathbf{f}}_i)} = -2\overline{\mathbf{S}}_i^{\mathrm{T}} \mathbf{V}_i (\Delta \mathbf{f}_i - \overline{\mathbf{S}}_i \, \mathrm{d}\overline{\mathbf{f}}_i) = -2(\overline{\mathbf{S}}_i^{\mathrm{T}} \mathbf{V}_i \Delta \mathbf{f}_i - \overline{\mathbf{S}}_i^{\mathrm{T}} \mathbf{V}_i \overline{\mathbf{S}}_i \, \mathrm{d}\overline{\mathbf{f}}_i) = \mathbf{0} \tag{16}$$

From this equation, we have

$$\mathrm{d}\bar{\mathbf{f}}_i = (\overline{\mathbf{S}}_i^{\mathrm{T}}\mathbf{V}_i\overline{\mathbf{S}}_i)^{-1}\overline{\mathbf{S}}_i^{\mathrm{T}}\mathbf{V}_i\Delta\mathbf{f}_i \tag{17}$$

In Eq. (17), it is observed that the number of supporting points m for each point i should be sufficiently large so as to ensure that the matrices $(\overline{\mathbf{S}}_i^{\mathrm{T}}\mathbf{V}_i\overline{\mathbf{S}}_i)$ are invertible at all points i in the domain Ω.

The final LSFD formulations can be derived from Eqs. (9b) and (17) as

$$\mathrm{d}\mathbf{f}_i = \mathbf{D}_i^{-1}(\overline{\mathbf{S}}_i^{\mathrm{T}}\mathbf{V}_i\overline{\mathbf{S}}_i)^{-1}\overline{\mathbf{S}}_i^{\mathrm{T}}\mathbf{V}_i\Delta\mathbf{f}_i \tag{18}$$

In order to simplify this formulation, the following matrices are defined:

$$\mathbf{T}^i = \mathbf{D}_i^{-1}(\overline{\mathbf{S}}_i^{\mathrm{T}}\mathbf{V}_i\overline{\mathbf{S}}_i)^{-1}(\overline{\mathbf{S}}_i^{\mathrm{T}}\mathbf{V}_i) \tag{19}$$

In view of Eq. (19), Eq. (18) may be rewritten as

$$\mathrm{d}\mathbf{f}_i = \mathbf{T}^i\Delta\mathbf{f}_i \tag{20}$$

where $\Delta\mathbf{f}_i$ and $\mathrm{d}\mathbf{f}_i$ are vectors given by expressions (10) and (4), respectively, and $\mathbf{T}^i \in R^{9\times m}$.

From the foregoing process, it is observed that for the 2D case, LSFD formulation (20) is derived by using the 2D Taylor series expansion with the first nine truncated terms. Higher-order LSFD schemes, which approximate derivatives of a function with a higher order of accuracy, can be derived by using the 2D Taylor series expansions with more terms. The formulations for higher-order LSFD schemes have the same form as Eq. (20).

The significance of the formulation (20) is that it expresses/approximates the derivatives at a point i with the forms of weighted summations of the function values at the point i itself and a set of its supporting points ij, for $j = 1,2,\ldots,m$. Any set of points i and ij, and even all the points in the problem domain, can be scattered. There is no specific connection between the points. Hence no mesh is required for discretization of the derivatives and PDEs. Furthermore, no meshing is required for solving the strong form of PDEs because there is no need for numerical integration. Therefore, this method is indeed mesh-free. As this method originates from a 2D Taylor series expansion (akin to the traditional FDM that originates from 1D Taylor series expansion) and the least-squares technique is adopted, this approach has been named the LSFD method.

3. Equations of motion for vibrating plates

For an isotropic, elastic thin plate with uniform thickness h, the longitudinal and rotary inertia forces can be assumed to be negligible. Accordingly, the equations of motion are given by [1]

$$\frac{\partial N_x}{\partial x} + \frac{\partial N_{xy}}{\partial y} = 0 \tag{21a}$$

$$\frac{\partial N_y}{\partial y} + \frac{\partial N_{xy}}{\partial x} = 0 \tag{21b}$$

$$D\nabla^4 w - \left(N_x\frac{\partial^2 w}{\partial x^2} + N_y\frac{\partial^2 w}{\partial y^2} + 2N_{xy}\frac{\partial^2 w}{\partial x\partial y}\right) = -\rho h\frac{\partial^2 w}{\partial t^2} \tag{21c}$$

where

$$D = \frac{Eh^3}{12(1-\nu^2)} \tag{22a}$$

$$N_x = B(\varepsilon_x + \nu\varepsilon_y) \tag{22b}$$

$$N_y = B(\varepsilon_y + \nu\varepsilon_x) \tag{22c}$$

$$N_{xy} = \frac{1-\nu}{2}B\gamma_{xy} \tag{22d}$$

$$B = \frac{Eh}{1 - v^2} \tag{22e}$$

$$\varepsilon_x = \frac{\partial u}{\partial x} + \frac{1}{2}\left(\frac{\partial w}{\partial x}\right)^2 \tag{22f}$$

$$\varepsilon_y = \frac{\partial v}{\partial y} + \frac{1}{2}\left(\frac{\partial w}{\partial y}\right)^2 \tag{22g}$$

$$\gamma_{xy} = \frac{\partial u}{\partial y} + \frac{\partial v}{\partial x} + \frac{\partial w}{\partial x}\frac{\partial w}{\partial y} \tag{22h}$$

In Eqs. (21) and (22), w is the lateral deflection, u and v the displacements of plate mid-surface elements in the x and y directions, ρ the mass density, t the time, D the flexural rigidity, E the Young modulus, v the Poisson ratio, B the extensional rigidity, N_x, N_y and N_{xy} the in-plane force components, ε_x, ε_y and γ_{xy} the in-plane strain components at the mid-surface of the plate.

4. Boundary conditions

The boundary conditions for the restrained edges considered herein are given below:

- Simply supported, immovable edge

$$w = 0, \quad \frac{\partial^2 w}{\partial n^2} + v\frac{\partial^2 w}{\partial s^2} = 0, \quad u = v = 0 \tag{23a,b,c}$$

- Clamped, immovable edge

$$w = 0, \quad \frac{\partial w}{\partial n} = 0, \quad u = v = 0 \tag{24a,b,c}$$

In Eqs. (23b) and (24b), n and s represent local coordinates normal and tangential, respectively, to the boundary at a boundary point.

5. Numerical solution

The substitution of Eqs. (22) into (21a,b) yields

$$\frac{\partial^2 u}{\partial x^2} + \frac{1-v}{2}\frac{\partial^2 u}{\partial y^2} + \frac{1+v}{2}\frac{\partial^2 v}{\partial x \partial y} = -\frac{\partial w}{\partial x}\left(\frac{\partial^2 w}{\partial x^2} + \frac{1-v}{2}\frac{\partial^2 w}{\partial y^2}\right) - \frac{1+v}{2}\frac{\partial w}{\partial y}\frac{\partial^2 w}{\partial x \partial y} \tag{25}$$

$$\frac{1+v}{2}\frac{\partial^2 u}{\partial x \partial y} + \frac{1-v}{2}\frac{\partial^2 v}{\partial x^2} + \frac{\partial^2 v}{\partial y^2} = -\frac{\partial w}{\partial y}\left(\frac{1-v}{2}\frac{\partial^2 w}{\partial x^2} + \frac{\partial^2 w}{\partial y^2}\right) - \frac{1+v}{2}\frac{\partial w}{\partial x}\frac{\partial^2 w}{\partial x \partial y} \tag{26}$$

For harmonic vibration, and by observing the relations between u, v, w implied in Eqs. (22f–h), (25) and (26), we can assume the expressions for u, v, w as

$$w(x, y, t) = W(x, y)H(t) \tag{27a}$$

$$u(x, y, t) = U(x, y)H^2(t) \tag{27b}$$

$$v(x, y, t) = V(x, y)H^2(t) \tag{27c}$$

where $W(x,y)$, $U(x,y)$ and $V(x,y)$ are the vibrating amplitudes of a plate element on the mid-surface in the transversal (z-) and longitudinal (x- and y-) directions, respectively, and they are merely functions of the 2D spatial coordinates (x, y); $H(t)$ is a periodic function of time.

By substituting Eqs. (27) into (25), (26) and (21c), and making use of Eqs. (22), we obtain

$$\frac{\partial^2 U}{\partial x^2}+\frac{1-v}{2}\frac{\partial^2 U}{\partial y^2}+\frac{1+v}{2}\frac{\partial^2 V}{\partial x\partial y}=-\frac{\partial W}{\partial x}\left(\frac{\partial^2 W}{\partial x^2}+\frac{1-v}{2}\frac{\partial^2 W}{\partial y^2}\right)-\frac{1+v}{2}\frac{\partial W}{\partial y}\frac{\partial^2 W}{\partial x\partial y} \tag{28a}$$

$$\frac{1+v}{2}\frac{\partial^2 U}{\partial x\partial y}+\frac{1-v}{2}\frac{\partial^2 V}{\partial x^2}+\frac{\partial^2 V}{\partial y^2}=-\frac{\partial W}{\partial y}\left(\frac{1-v}{2}\frac{\partial^2 W}{\partial x^2}+\frac{\partial^2 W}{\partial y^2}\right)-\frac{1+v}{2}\frac{\partial W}{\partial x}\frac{\partial^2 W}{\partial x\partial y} \tag{28b}$$

$$(\nabla^4 W)H(t)-\frac{12}{h^2}\left(\begin{array}{c}\left(\frac{\partial U}{\partial x}+\frac{1}{2}\left(\frac{\partial W}{\partial x}\right)^2+v\left[\frac{\partial V}{\partial y}+\frac{1}{2}\left(\frac{\partial W}{\partial y}\right)^2\right]\right)\frac{\partial^2 W}{\partial x^2}\\ +\left(\frac{\partial V}{\partial y}+\frac{1}{2}\left(\frac{\partial W}{\partial y}\right)^2+v\left[\frac{\partial U}{\partial x}+\frac{1}{2}\left(\frac{\partial W}{\partial x}\right)^2\right]\right)\frac{\partial^2 W}{\partial y^2}\\ +(1-v)\left(\frac{\partial U}{\partial y}+\frac{\partial V}{\partial x}+\frac{\partial W}{\partial x}\frac{\partial W}{\partial y}\right)\frac{\partial^2 W}{\partial x\partial y}\end{array}\right)H^3(t)$$
$$=-\lambda_L^2\frac{W}{a^4\omega_L^2}\frac{\mathrm{d}^2H(t)}{\mathrm{d}t^2} \tag{28c}$$

where

$$\lambda_L=\omega_L a^2\sqrt{\frac{\rho h}{D}} \tag{29}$$

is the frequency parameter of the linear small-amplitude free vibration of a plate, ω_L the corresponding angular frequency, and a the characteristic length of the plate. If one converts the time quantity t into a nondimensional time quantity τ and transforms the temporal function $H(t)$ into $\overline{H}(\tau)$ such that

$$\tau=\omega_L t \tag{30}$$

$$H(t)=H\left(\frac{\tau}{\omega_L}\right)=\overline{H}(\tau) \tag{31}$$

then Eq. (28c) can be transformed into the form

$$(\nabla^4 W)\overline{H}(\tau)-\frac{12}{h^2}\left(\begin{array}{c}\left(\frac{\partial U}{\partial x}+\frac{1}{2}\left(\frac{\partial W}{\partial x}\right)^2+v\left[\frac{\partial V}{\partial y}+\frac{1}{2}\left(\frac{\partial W}{\partial y}\right)^2\right]\right)\frac{\partial^2 W}{\partial x^2}\\ +\left(\frac{\partial V}{\partial y}+\frac{1}{2}\left(\frac{\partial W}{\partial y}\right)^2+v\left[\frac{\partial U}{\partial x}+\frac{1}{2}\left(\frac{\partial W}{\partial x}\right)^2\right]\right)\frac{\partial^2 W}{\partial y^2}\\ +(1-v)\left(\frac{\partial U}{\partial y}+\frac{\partial V}{\partial x}+\frac{\partial W}{\partial x}\frac{\partial W}{\partial y}\right)\frac{\partial^2 W}{\partial x\partial y}\end{array}\right)\overline{H}^3(\tau)$$
$$=-\lambda_L^2\frac{W}{a^4}\frac{\mathrm{d}^2\overline{H}(\tau)}{\mathrm{d}\tau^2} \tag{32}$$

Eq. (32) can be regarded as an ODE of the function $\overline{H}(\tau)$, and it should be satisfied everywhere in the plate domain theoretically. As pointed out by Chu and Herrmann [4] and Wah [7], the effects of in-plane forces on the mode shapes $W(x,y)$ and the effects of coupling of different modes can be neglected in large-amplitude free vibration of plates. Therefore, $W(x,y)$ in Eq. (32) can be determined from the mode shapes of the small-amplitude free vibration when its frequency parameter is λ_L, i.e., $W(x,y)$ and λ_L can be solved from the linear differential equation [3]

$$\nabla^4 W = \frac{\lambda_L^2}{a^4} W \tag{33}$$

By using the LSFD formulation (20), the left-hand side of Eq. (33) can be discretized at an interior point i as

$$\nabla^4 W_i = \sum_{j=1}^{m} T^i_{(\nabla^2),j}(\nabla^2 W_{ij} - \nabla^2 W_i) \tag{34}$$

where $T^i_{(\nabla^2),j} = T^i_{3,j} + T^i_{4,j}$, and $T^i_{3,j}$, $T^i_{4,j}$ are the elements of the third row and fourth row of the coefficient matrix $\mathbf{T}^i$. If the point ij is on a straight simply supported edge, then the boundary condition $\nabla^2 W_{ij} = 0$ can be substituted into Eq. (34). If the point ij is on a curved simply supported edge, then the boundary condition $\nabla^2 W_{ij} = \pm[(1-v)/r_{ij}](\partial W_{ij}/\partial n)$ can be substituted into Eq. (34), where the positive sign is for convex edge, the negative sign for concave edge, r_{ij} the radius of curvature of the edge curve at point ij and $\partial W_{ij}/\partial n$ the slope of W in the normal direction to the edge at point ij [17]. If the point ij is on a clamped edge, then $\nabla^2 W_{ij}$ in Eq. (34) can be further discretized as

$$\nabla^2 W_{ij} = \frac{\partial^2 W_{ij}}{\partial x^2} + \frac{\partial^2 W_{ij}}{\partial y^2} = \sum_{k=1}^{m} T^{ij}_{1,k}\left(\frac{\partial W_{ijk}}{\partial x} - \frac{\partial W_{ij}}{\partial x}\right) + \sum_{k=1}^{m} T^{ij}_{2,k}\left(\frac{\partial W_{ijk}}{\partial y} - \frac{\partial W_{ij}}{\partial y}\right) \tag{35}$$

and the boundary conditions $\partial W_{ij}/\partial x = 0$, $\partial W_{ij}/\partial y = 0$ can be substituted into Eq. (35) as well as into Eq. (34). After implementing one boundary condition of simply supported or clamped edge, the remaining derivatives in the right-hand side of Eq. (34) can be further discretized into a form of weighted summation of the function values of W at a group of points. If any boundary point is involved in this summation, the boundary condition $W = 0$ for simply supported or clamped edges can be implemented. Finally, Eq. (33), which is collocated at all interior points $i = 1,\ldots,n$, can be discretized into the following system of algebraic equations:

$$\mathbf{A}\mathbf{w} = \frac{\lambda_L^2}{a^4}\mathbf{w} \tag{36}$$

where $\mathbf{A} \in R^{n\times n}$, $\mathbf{w} = [W_1 \ldots W_n]^{\mathrm{T}}$. The linear frequency parameters λ_L and mode shapes $\mathbf{w}$ can be derived by solving the eigenvalues and eigenvectors of the matrix $\mathbf{A}$.

Upon the availability of linear vibration mode shapes $\mathbf{w}$, the large-amplitude vibration mode shapes can be derived by proper scaling of the vector $\mathbf{w}$. The displacements U and V can then be solved from Eqs. (28a, b) and necessary boundary conditions, which are given by $U|_\Gamma = V|_\Gamma = 0$ for the immovable condition at the plate edge Γ.

Numerically, one can calculate the coefficients in Eq. (32) as follows:

$$\left[\sum_{i=1}^{n}(\nabla^4 W_i)\right]\overline{H}(\tau) - \left\{\sum_{i=1}^{n}\frac{12}{h^2}\left(\begin{array}{c}\left(\frac{\partial U_i}{\partial x} + \frac{1}{2}\left(\frac{\partial W_i}{\partial x}\right)^2 + v\left[\frac{\partial V_i}{\partial y} + \frac{1}{2}\left(\frac{\partial W_i}{\partial y}\right)^2\right]\right)\frac{\partial^2 W_i}{\partial x^2} \\ + \left(\frac{\partial V_i}{\partial y} + \frac{1}{2}\left(\frac{\partial W_i}{\partial y}\right)^2 + v\left[\frac{\partial U_i}{\partial x} + \frac{1}{2}\left(\frac{\partial W_i}{\partial x}\right)^2\right]\right)\frac{\partial^2 W_i}{\partial y^2} \\ +(1-v)\left(\frac{\partial U_i}{\partial y} + \frac{\partial V_i}{\partial x} + \frac{\partial W_i}{\partial x}\frac{\partial W_i}{\partial y}\right)\frac{\partial^2 W_i}{\partial x \partial y}\end{array}\right)\right\}\overline{H}^3(\tau)$$
$$= -\frac{\lambda_L^2}{a^4}\left(\sum_{i=1}^{n} W_i\right)\frac{\mathrm{d}^2\overline{H}(\tau)}{\mathrm{d}\tau^2} \tag{37}$$

Eq. (37) can be simplified to the form

$$\frac{\mathrm{d}^2\overline{H}(\tau)}{\mathrm{d}\tau^2} = \alpha\overline{H}(\tau) + \beta\overline{H}^3(\tau) \tag{38}$$

where

$$\alpha = -\left[\sum_{i=1}^{n}(\nabla^4 W_i)\right] \Bigg/ \left(\frac{\lambda_L^2}{a^4}\sum_{i=1}^{n} W_i\right) \tag{39}$$

$$\beta = \frac{12a^4}{h^2\lambda_L^2\sum_{i=1}^{n} W_i}\sum_{i=1}^{n}\left(\begin{array}{c} \left(\frac{\partial U_i}{\partial x}+\frac{1}{2}\left(\frac{\partial W_i}{\partial x}\right)^2+v\left[\frac{\partial V_i}{\partial y}+\frac{1}{2}\left(\frac{\partial W_i}{\partial y}\right)^2\right]\right)\frac{\partial^2 W_i}{\partial x^2} \\ +\left(\frac{\partial V_i}{\partial y}+\frac{1}{2}\left(\frac{\partial W_i}{\partial y}\right)^2+v\left[\frac{\partial U_i}{\partial x}+\frac{1}{2}\left(\frac{\partial W_i}{\partial x}\right)^2\right]\right)\frac{\partial^2 W_i}{\partial y^2} \\ +(1-v)\left(\frac{\partial U_i}{\partial y}+\frac{\partial V_i}{\partial x}+\frac{\partial W_i}{\partial x}\frac{\partial W_i}{\partial y}\right)\frac{\partial^2 W_i}{\partial x\partial y} \end{array}\right) \tag{40}$$

From Eqs. (39) and (40), it is observed that the determination of α and β requires the condition of $\sum_{i=1}^{n} W_i \neq 0$. However, for some vibration modes, $\sum_{i=1}^{n} W_i$ tends to be zero. In such cases, one can keep the original form of Eq. (32) which collocates at points where $W_i \geqslant 0$ and swap the signs of Eq. (32) which collocates at points where $W_i < 0$, and then summing them together to form an equation that is similar to Eq. (37).

In Eq. (40), the low order derivatives of U, V, W can be calculated by using the formulation (20) directly. The high-order derivative $\nabla^4 W_i$ can be calculated by using following discretization:

$$\begin{aligned} \nabla^4 W_i &= \sum_{j=1}^{m} T^i_{(\nabla^2),j}(\nabla^2 W_{ij} - \nabla^2 W_i) \\ &= \sum_{j=1}^{m} T^i_{(\nabla^2),j}\left[\sum_{k=1}^{m} T^{ij}_{(\nabla^2),k}(W_{ijk} - W_{ij}) - \sum_{j=1}^{m} T^i_{(\nabla^2),j}(W_{ij} - W_i)\right] \end{aligned} \tag{41}$$

In order to solve Eq. (38), two initial conditions are needed and they are

$$(\overline{H})_{\tau=0} = 1, \quad \left(\frac{\mathrm{d}(\overline{H})}{\mathrm{d}\tau}\right)_{\tau=0} = 0 \tag{42a,b}$$

Eq. (38) can be solved numerically by using the finite difference method. The procedural steps are as follows:

Step 1: Set a time increment $\Delta\tau$.

Step 2: When $\tau = 0$,

$$(\ddot{\overline{H}})_{\tau=0} = \alpha(\overline{H})_{\tau=0} + \beta(\overline{H}^3)_{\tau=0} = \alpha + \beta \tag{43a}$$

$$\rightarrow \frac{(\overline{H})_{\tau=\Delta\tau} - 2(\overline{H})_{\tau=0} + (\overline{H})_{\tau=-\Delta\tau}}{(\Delta\tau)^2} = \frac{2(\overline{H})_{\tau=\Delta\tau} - 2(\overline{H})_{\tau=0}}{(\Delta\tau)^2} = \alpha + \beta \tag{43b}$$

$$\rightarrow (\overline{H})_{\tau=\Delta\tau} = (\overline{H})_{\tau=0} + \tfrac{1}{2}(\Delta\tau)^2(\alpha+\beta) = 1 + \tfrac{1}{2}(\Delta\tau)^2(\alpha+\beta) \tag{43c}$$

Step 3: For $j = 1,2,3,\ldots,$

$$(\ddot{\overline{H}})_{\tau=j\Delta\tau} = \alpha(\overline{H})_{\tau=j\Delta\tau} + \beta(\overline{H}^3)_{\tau=j\Delta\tau} \tag{44a}$$

$$\rightarrow \frac{(\overline{H})_{\tau=(j+1)\Delta\tau} - 2(\overline{H})_{\tau=j\Delta\tau} + (\overline{H})_{\tau=(j-1)\Delta\tau}}{(\Delta\tau)^2} = \alpha(\overline{H})_{\tau=j\Delta\tau} + \beta(\overline{H}^3)_{\tau=j\Delta\tau} \tag{44b}$$

$$(\overline{H})_{\tau=(j+1)\Delta\tau} = 2(\overline{H})_{\tau=j\Delta\tau} - (\overline{H})_{\tau=(j-1)\Delta\tau} + (\Delta\tau)^2[\alpha(\overline{H})_{\tau=j\Delta\tau} + \beta(\overline{H})^3_{\tau=j\Delta\tau}] \tag{44c}$$

Step 4: Plot $\overline{H}(\tau)$ curve or observe the data result of $\overline{H}(\tau)$ for the period T_{NL}. For example, if we find the period of τ of the function $\overline{H}(\tau)$ is

$$\omega_L T_{\mathrm{NL}} = k2\pi \tag{45}$$

and since $\omega_L T_L = 2\pi$, then the ratio of the nonlinear vibration period to the linear vibration period is

$$T_{\mathrm{NL}}/T_L = k \tag{46}$$

6. Results and discussion

By using the LSFD method, the linear frequency parameters (λ_L), normalized mode shapes ($\overline{W}:\overline{W} \equiv W/W_{\max}$), and nonlinear-to-linear period ratios (T_{NL}/T_L) are obtained for various plate shapes and boundary conditions. The effect of large vibrating amplitudes on the vibrating frequencies or periods is indicated by the ratios T_{NL}/T_L that change with the relative vibrating amplitudes $W_{\max}/h$. In order to confirm the accuracy and availability of the LSFD method, the convergence study of LSFD solutions are performed by increasing the number of points in the plate domain and by adopting different orders of LSFD schemes. For all cases, we adopt the LSFD formulations given by Eq. (20) that are derived from the Taylor series expansions (1) with 20 and 27 truncated terms. The LSFD solutions are compared with exact or approximate solutions (if available) from other sources. The versatility of the LSFD method is established by the fact that the method is able to furnish accurate solutions for higher vibration modes, arbitrary plate shapes and various boundary conditions.

In Table 1, the LSFD linear frequency parameters λ_L and period ratios T_{NL}/T_L of the first three vibration modes of a simply supported square plate are presented. We have used two random distributions of points in the square domain (i.e. 441 points and 1156 points) and the aforementioned two LSFD schemes to study the convergence behavior of the LSFD solutions. It is observed that the λ_L values obtained by LSFD for all the three modes converge to the exact values [3] when the number of points increases and the higher-order LSFD scheme is adopted. The T_{NL}/T_L values corresponding to the relative vibrating amplitudes $W_{\max}/h = 0$, 0.2, 0.4, 0.6, 0.8 and 1.0 are presented in Table 1. The effect of large vibrating amplitude on the period of the plate can be observed clearly; i.e., when the vibrating amplitude becomes larger, the vibration of plate tends to be faster due to the presence of larger stretching in-plane forces generated in the plate. These T_{NL}/T_L values also converge well and they agree closely with the results obtained by Chu and Herrmann [4], Wah [7], Mei [8] and Rao et al. [9].

In Section 5, we expect that the coefficients in Eq. (32) can be calculated by using the form of Eq. (37); i.e., in order to get the global vibration characteristics of the plate, we wish to collocate Eq. (32) at all the interior points on the plate domain and then summing them up. However, by performing this operation, it is found that the ratio T_{NL}/T_L does not approach the expected value of 1.0 as the relative vibrating amplitude $W_{\max}/h$ approaches zero. One realizes that Eq. (32) should be satisfied everywhere on the plate domain theoretically, but from a numerical standpoint, the solutions to W, U and V obtained in the vicinity of the plate edges may not be sufficiently accurate. This inaccuracy causes the coefficients of Eq. (32) collocating at points near plate edges to deviate too much from the exact values, and finally leads to large errors in the summation form of Eq. (37). This problem may be overcome by employing the following measure. For each plate case, we can find a constant $c{:}0<c<1$ via a numerical test such that

$$T_{\mathrm{NL}}/T_L \to 1.0 \;\text{ as }\; W_{\max}/h \to 0$$

by collocating Eq. (32) only at points i where $|W_i| \geqslant c|W_{\max}|$ and taking the resulting equations into account in the summation form of Eq. (37).

The LSFD normalized mode shapes ($\overline{W}$) of the first three free vibration modes of the simply supported square plate are presented in Fig. 2. We can observe that for the first mode, $W>0$ for the whole interior domain of plate. For this case, the summation form of Eq. (37) can be directly formed without swapping the signs of Eq. (32) collocated at interior points before the summation is done. However, for the second and third modes, $W>0$ for half area of the plate, but $W<0$ in the other half. For these two cases, $\sum_{i=1}^{n} W_i$ tends to zero

Table 1
Linear frequency parameters ($\lambda_L = \omega_L a^2 \sqrt{\rho h/D}$) and period ratios ($T_{NL}/T_L$) of a simply supported square plate ($a = 1$)

Number of points	Order of scheme[a]	λ_L	W_{max}/h					
			0	0.2	0.4	0.6	0.8	1.0
LSFD			*Fundamental mode*					
441	20	19.7344	1.0	0.9827	0.9359	0.8713	0.8003	0.7307
441	27	19.7393	1.0	0.9827	0.9360	0.8715	0.8006	0.7310
1156	20	19.7386	1.0	0.9827	0.9360	0.8715	0.8007	0.7311
1156	27	19.7392	1.0	0.9827	0.9360	0.8715	0.8007	0.7312
Rao et al. [9]		–	1.0	0.9818	0.9331	0.8670	0.7958	0.7271
Mei [8]		–	1.0	0.9821	0.9338	0.8673	0.7943	0.7233
Chu and Herrmann [4]		–	1.0	0.9809	0.9297	0.8602	0.7853	0.7131
Wah [7]		–	1.0	0.9783	0.9210	0.8451	0.7653	0.6901
Leissa [3]		19.7392[b]	–	–	–	–	–	–
LSFD			*Second mode*					
441	20	49.2781	1.0	0.9785	0.9219	0.8467	0.7673	0.6924
441	27	49.3479	1.0	0.9813	0.9314	0.8632	0.7894	0.7178
1156	20	49.3388	1.0	0.9793	0.9246	0.8514	0.7735	0.6995
1156	27	49.3480	1.0	0.9813	0.9313	0.8631	0.7892	0.7177
Rao et al. [9]		–	1.0	0.9773	0.9182	0.8393	0.7564	0.6786
Leissa [3]		49.3480[b]	–	–	–	–	–	–
LSFD			*Third mode*					
441	20	78.6596	1.0	0.9820	0.9337	0.8673	0.7950	0.7244
441	27	78.9615	1.0	0.9825	0.9352	0.8701	0.7988	0.7289
1156	20	78.9155	1.0	0.9824	0.9350	0.8697	0.7982	0.7282
1156	27	78.9568	1.0	0.9825	0.9352	0.8701	0.7987	0.7288
Rao et al. [9]		–	1.0	0.9825	0.9353	0.8704	0.7996	0.7305
Leissa [3]		78.9568[b]	–	–	–	–	–	–

[a]Number of truncated terms in Eq. (1).
[b]Exact values.

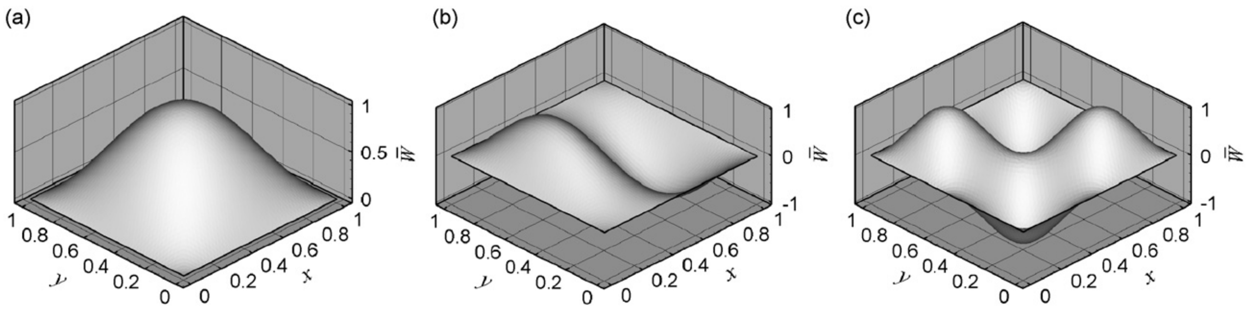

Fig. 2. Free vibration mode shapes of a SSSS square plate: (a) first mode, (b) second mode and (c) third mode.

obviously. We need to keep the original form of Eq. (32) which collocates at points where $W_i \geqslant 0$ and swap the signs of Eq. (32) which collocates at points where $W_i < 0$, and then summing them up to form an equation that is similar to Eq. (37).

Table 2 and Fig. 3 present the LSFD linear frequency parameters λ_L, period ratios T_{NL}/T_L, and normalized mode shapes $\overline{W}$ of a clamped square plate for the first three vibration modes. Two point distributions

Table 2
Linear frequency parameters ($\lambda_L = \omega_L a^2 \sqrt{\rho h/D}$) and period ratios ($T_{NL}/T_L$) of a clamped square plate ($a = 1$)

Number of points	Order of scheme	λ_L	W_{max}/h					
			0	0.2	0.4	0.6	0.8	1.0
LSFD			*Fundamental mode*					
441	20	35.9564	1.0	0.9929	0.9723	0.9409	0.9018	0.8582
441	27	35.9732	1.0	0.9915	0.9672	0.9307	0.8861	0.8374
1156	20	35.9812	1.0	0.9941	0.9770	0.9504	0.9168	0.8785
1156	27	35.9847	1.0	0.9941	0.9770	0.9505	0.9169	0.8787
Rao et al. [9]		–	1.0	0.9930	0.9731	0.9427	0.9052	0.8637
Mei [8]		–	1.0	0.9938	0.9750	0.9466	0.9116	0.8750
Yamaki [5]		–	1.0	0.9916	0.9716	0.9380	0.8980	0.8566
Leissa [3]		35.982[a] 35.986[b]	–	–	–	–	–	–
LSFD			*Second mode*					
441	20	73.1904	1.0	0.9859	0.9473	0.8921	0.8294	0.7656
441	27	73.3525	1.0	0.9840	0.9404	0.8796	0.8117	0.7443
1156	20	73.3636	1.0	0.9891	0.9583	0.9132	0.8598	0.8035
1156	27	73.3908	1.0	0.9879	0.9541	0.9050	0.8478	0.7884
Rao et al. [9]		–	1.0	0.9860	0.9478	0.8942	0.8337	0.7725
Leissa [3]		73.40[c]	–	–	–	–	–	–
LSFD			*Third mode*					
441	20	107.461	1.0	0.9840	0.9405	0.8796	0.8118	0.7444
441	27	108.063	1.0	0.9829	0.9365	0.8723	0.8018	0.7325
1156	20	108.106	1.0	0.9879	0.9541	0.9051	0.8480	0.7887
1156	27	108.203	1.0	0.9879	0.9541	0.9050	0.8478	0.7884
Rao et al. [9]		–	1.0	0.9870	0.9514	0.9015	0.8451	0.7880
Leissa [3]		108.22[c]	–	–	–	–	–	–

[a]Lower bound value.
[b]Upper bound value.
[c]Values from Table 4.22 in Leissa [3].

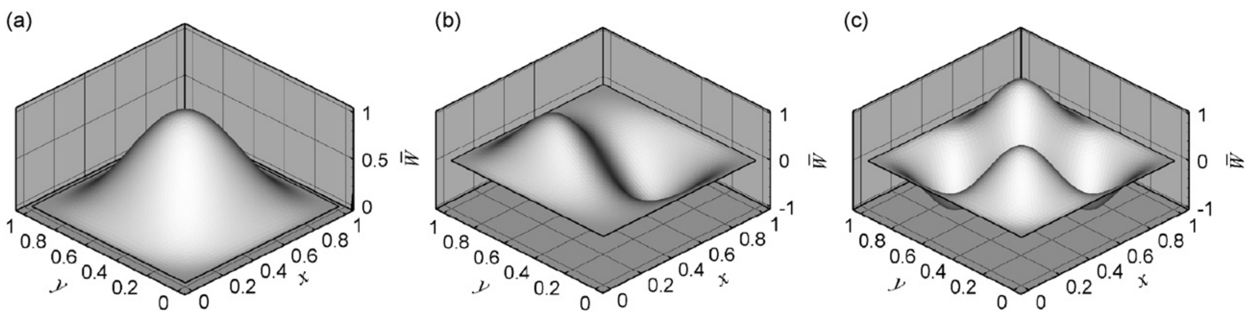

Fig. 3. Free vibration mode shapes of a CCCC square plate: (a) first mode, (b) second mode and (c) third mode.

(441 points and 1156 points) and the two LSFD schemes are adopted to study the convergence behaviors of the LSFD solutions. In Table 2, it can be seen that the λ_L values obtained by LSFD for all the three modes are in very close agreement with the data presented in Leissa [3]. The T_{NL}/T_L values also agree well with the data

Table 3
Linear frequency parameters ($\lambda_L = \omega_L a^2 \sqrt{\rho h/D}$) and period ratios ($T_{NL}/T_L$) for the fundamental modes of a square plate ($a = 1$) with different boundary conditions

Number of points	Order of scheme	λ_L	W_{max}/h					
			0	0.2	0.4	0.6	0.8	1.0
LSFD			*SSCC plate*					
441	20	27.0418	1.0	0.9873	0.9522	0.9014	0.8426	0.7819
441	27	27.0530	1.0	0.9874	0.9523	0.9017	0.8431	0.7825
1156	20	27.0523	1.0	0.9896	0.9605	0.9174	0.8660	0.8114
1156	27	27.0541	1.0	0.9897	0.9605	0.9174	0.8661	0.8116
Rao et al. [9]		–	1.0	0.9864	0.9499	0.8994	0.8435	0.7871
Mei [8]		–	1.0	0.985	0.960	0.912	0.860	0.806
Leissa [3]		27.10	–	–	–	–	–	–
LSFD			*SCSC plate*					
441	20	28.9379	1.0	0.9889	0.9578	0.9122	0.8584	0.8018
441	27	28.9502	1.0	0.9890	0.9581	0.9127	0.8591	0.8027
1156	20	28.9491	1.0	0.9912	0.9664	0.9290	0.8834	0.8339
1156	27	28.9508	1.0	0.9913	0.9664	0.9290	0.8835	0.8341
Rao et al. [9]		–	1.0	0.9904	0.9634	0.9231	0.8750	0.8235
Mei [8]		–	1.0	0.9919	0.9675	0.9307	0.8858	0.8370
Leissa [3]		28.946	–	–	–	–	–	–
LSFD			*CCCS plate*					
441	20	31.8061	1.0	0.9896	0.9604	0.9173	0.8658	0.8112
441	27	31.8212	1.0	0.9897	0.9607	0.9178	0.8666	0.8122
1156	20	31.8234	1.0	0.9931	0.9733	0.9430	0.9050	0.8626
1156	27	31.8258	1.0	0.9923	0.9704	0.9370	0.8958	0.8502
Rao et al. [9]		–	1.0	0.9907	0.9646	0.9262	0.8807	0.8322
Mei [8]		–	1.0	0.994	0.975	0.944	0.905	0.865
Leissa [3]		31.83	–	–	–	–	–	–
LSFD			*SSSC plate*					
441	20	23.6385	1.0	0.9861	0.9476	0.8928	0.8304	0.7668
441	27	23.6463	1.0	0.9852	0.9445	0.8870	0.8221	0.7568
1156	20	23.6453	1.0	0.9870	0.9508	0.8989	0.8390	0.7774
1156	27	23.6463	1.0	0.9870	0.9509	0.8989	0.8390	0.7775
Rao et al. [9]		–	1.0	0.9848	0.9440	0.8877	0.8258	0.7645
Mei [8]		–	1.0	0.984	0.954	0.900	0.844	0.784
Leissa [3]		23.646	–	–	–	–	–	–

obtained by Yamaki [5], Mei [8] and Rao et al. [9]. The first three mode shapes of this clamped square plate are similar to those of the simply supported square plate. The difference between them is that for the simply supported square plate, the slope of the transverse deflection, $\partial W/\partial n$, is nonzero whereas for the clamped square plate, $\partial W/\partial n$ is constrained to be zero along the plate edges.

In the foregoing problems, all the plate edges are either simply supported or clamped. Next we consider square plates with a combination of simply supported and clamped edges. Table 3 and Fig. 4 present linear frequency parameters λ_L, period ratios T_{NL}/T_L, and normalized mode shapes $\overline{W}$ for the fundamental modes of square plates with four combinations of boundary conditions, i.e. SSCC, SCSC, CCCS and SSSC. We can observe that the LSFD results for λ_L and T_{NL}/T_L values converge well and are in good agreement with the data from previous researchers [3,8,9].

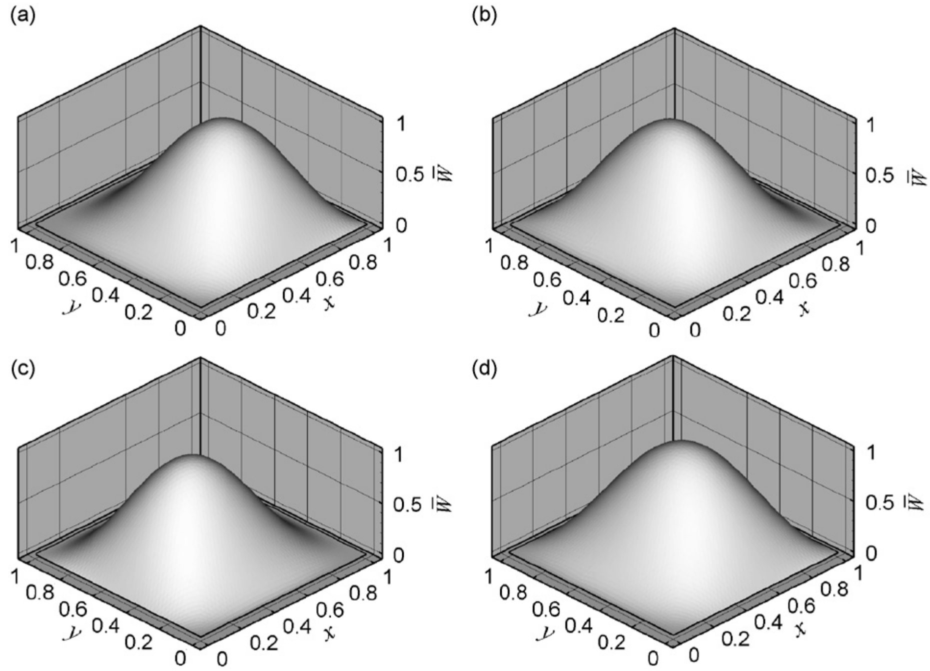

Fig. 4. Fundamental mode shapes of a square plate: (a) SSCC plate, (b) SCSC plate, (c) CCCS plate and (d) SSSC plate.

Table 4
Linear frequency parameters ($\lambda_L = \omega_L R^2\sqrt{\rho h/D}$) and period ratios ($T_{NL}/T_L$) for the fundamental modes of a circular plate ($R = 1$)

Number of points	Order of scheme	λ_L	W_{max}/h					
			0	0.2	0.4	0.6	0.8	1.0
LSFD			*Simply supported plate*					
629	20	4.9349	1.0	0.9740	0.9073	0.8219	0.7354	0.6565
629	27	4.9351	1.0	0.9730	0.9038	0.8162	0.7282	0.6486
1237	20	4.9351	1.0	0.9745	0.9087	0.8243	0.7384	0.6598
1237	27	4.9351	1.0	0.9740	0.9071	0.8216	0.7351	0.6561
Mei et al. [11]		4.946	1.0	0.9748	0.9104	0.8284	0.7460	0.6713
Yamaki [5]		4.947	1.0	0.9734	0.9052	0.8185	0.7312	0.6518
Rao et al. [10]		–	1.0	0.9744	0.9089	0.8261	0.7432	0.6682
Leissa [3]		4.977	–	–	–	–	–	–
LSFD			*Clamped plate*					
629	20	10.214	1.0	0.9942	0.9774	0.9512	0.9180	0.8802
629	27	10.216	1.0	0.9934	0.9745	0.9453	0.9087	0.8676
1237	20	10.215	1.0	0.9949	0.9800	0.9568	0.9269	0.8925
1237	27	10.216	1.0	0.9949	0.9801	0.9568	0.9270	0.8926
Mei et al. [11]		10.144	1.0	0.9929	0.9724	0.9414	0.9031	0.8609
Yamaki [5]		10.327	1.0	0.9930	0.9730	0.9422	0.9038	0.8608
Rao et al. [10]		–	1.0	0.9928	0.9724	0.9413	0.9029	0.8607
Leissa [3]		10.216	–	–	–	–	–	–

Next, we consider the large-amplitude vibration of a circular plate as a typical example of a plate with curved edges. Table 4 and Fig. 5 present λ_L, T_{NL}/T_L and $\overline{W}$ for the fundamental modes of simply supported and clamped circular plates. For both boundary conditions, the convergence studies of the LSFD solutions

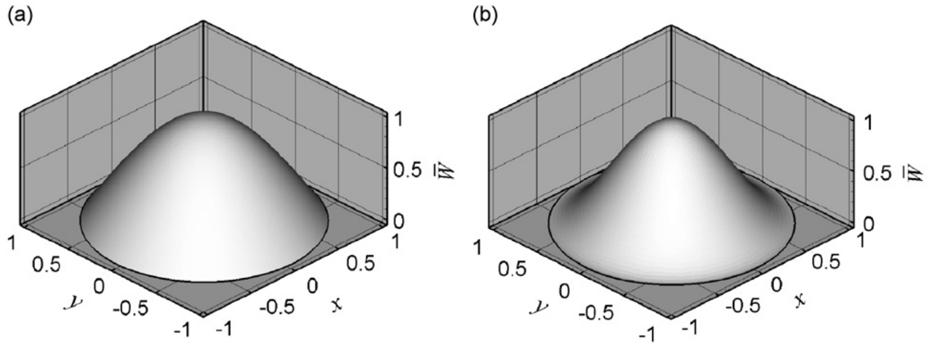

Fig. 5. Fundamental mode shapes of a circular plate: (a) simply supported and (b) clamped.

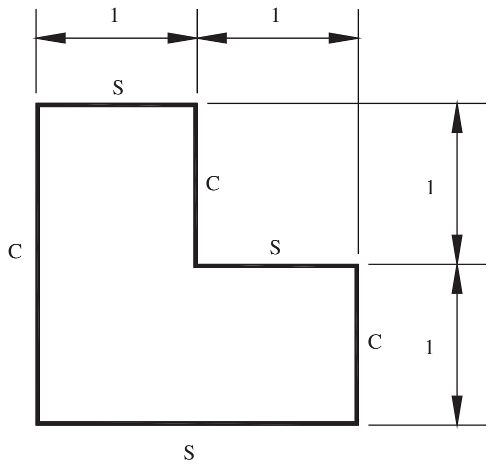

Fig. 6. Geometry and support conditions of an L-shaped plate.

were performed by using two point distributions (629 points and 1237 points) and the two orders of LSFD schemes. It can be seen from Table 4 that all the LSFD solutions for the circular plate are in good agreement with the results obtained by Leissa [3], Yamaki [5], Rao et al. [10] and Mei et al. [11]. The accurate LSFD results confirm that the LSFD method can be conveniently used for tackling plates with curve edges.

Previous example problems of square and circular plates can be regarded as problems involving simple convex domains. What about plates with a concave domain? Such a problem is more difficult to solve accurately by using a numerical method. For example, one cannot approximate the plate deflection functions accurately within a concave domain by using the Ritz method with global Ritz functions. Compared to the Ritz method, the LSFD method possesses two features: (1) mesh-free, i.e. approximation and discretization of functions, derivatives and PDEs are based on scattered points in problem domains; (2) local approximation, i.e. approximation and discretization of derivatives are performed in local, much smaller regions (compared to a global domain) of a domain. These two features allow the LSFD method to accommodate problems with complex domain shapes, such as concave domains and multi-connected domains. In order to assess the performance of the LSFD method in handling large-amplitude vibration plate problems with concave domains, we consider an L-shaped plate and a square plate with semi-circular edge cuts.

Fig. 6 shows the geometry and support conditions of the L-shaped plate. In Table 5 and Fig. 7, the LSFD linear frequency parameters λ_L, period ratios T_{NL}/T_L and the normalized mode shapes $\overline{W}$ for the first three vibration modes of this plate shape are presented. The convergence study of the LSFD solutions is carried out by using two distributions of points (814 points and 1433 points) and the two LSFD schemes. It can be

Table 5
Linear frequency parameters ($\lambda_L = \omega_L a^2 \sqrt{\rho h/D}$) and period ratios ($T_{NL}/T_L$) of the L-shaped plate ($a = 2$)

Number of points	Order of scheme	λ_L	W_{max}/h					
			0	0.2	0.4	0.6	0.8	1.0
LSFD			*Fundamental mode*					
814	20	59.131	1.0	0.9853	0.9449	0.8878	0.8233	0.7582
814	27	58.529	1.0	0.9844	0.9420	0.8823	0.8156	0.7489
1433	20	59.136	1.0	0.9893	0.9592	0.9148	0.8623	0.8066
1433	27	59.055	1.0	0.9892	0.9590	0.9145	0.8617	0.8060
Shi and Mei [13]		–	–	0.9852	0.9470	0.8937	0.8361	0.7788
Kurpa et al. [14]	RFM(a)	–	–	0.9862	0.9497	0.8977	0.8382	0.7770
	RFM(b)	–	–	0.9901	0.9606	0.9174	0.8651	0.8097
LSFD			*Second mode*					
814	20	86.072	1.0	0.9830	0.9369	0.8732	0.8029	0.7338
814	27	86.876	1.0	0.9818	0.9330	0.8660	0.7932	0.7223
1433	20	86.735	1.0	0.9878	0.9539	0.9047	0.8474	0.7878
1433	27	86.746	1.0	0.9869	0.9505	0.8982	0.8380	0.7762
LSFD			*Third mode*					
814	20	105.711	1.0	0.9854	0.9452	0.8883	0.8239	0.7590
814	27	106.123	1.0	0.9854	0.9454	0.8886	0.8244	0.7596
1433	20	106.185	1.0	0.9907	0.9642	0.9246	0.8769	0.8254
1433	27	106.229	1.0	0.9901	0.9621	0.9204	0.8706	0.8173

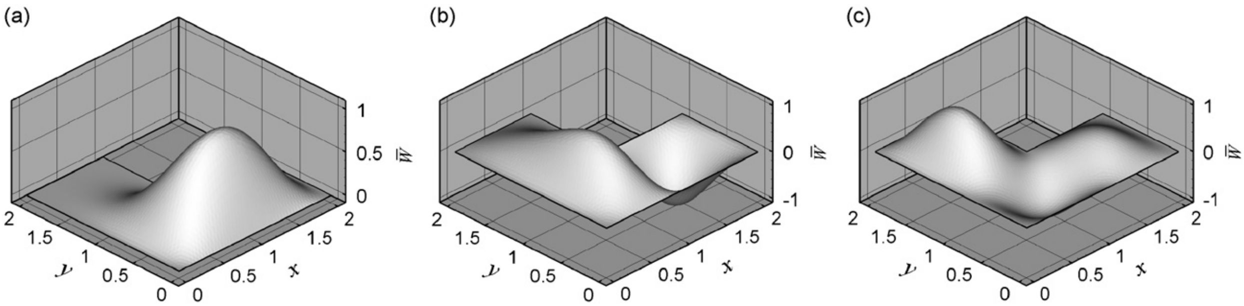

Fig. 7. Free vibration mode shapes of the L-shaped plate with boundary conditions shown in Fig. 6: (a) first mode, (b) second mode and (c) third mode.

observed that both λ_L and T_{NL}/T_L values converged, and T_{NL}/T_L values agree well with those obtained by Shi and Mei [13] and Kurpa et al. [14].

Fig. 8 shows the geometry of the square plate with semi-circular edge cuts. The large-amplitude vibration of this plate with simply supported and clamped edges is analyzed by using the LSFD method. It can be seen that the four corner regions are connected to the central region of the plate by narrow "passageways". We can imagine that in order to solve this problem correctly and accurately, a numerical method must be able to correctly and accurately transform information among all the corner regions and the central region. Such a requirement may pose difficulties for some numerical methods such as the Ritz method.

Presented in Tables 6 and 7 as well as Figs. 9 and 10 are the linear frequency parameters λ_L, nonlinear-to-linear period ratios T_{NL}/T_L, and normalized mode shapes $\overline{W}$ for the first three vibration modes of the simply supported and clamped square plates with semi-circular edge cuts. For each boundary condition, three distributions of points (1020, 1552 and 2445 points for simply supported plate; 1020, 1552 and 2916 points for

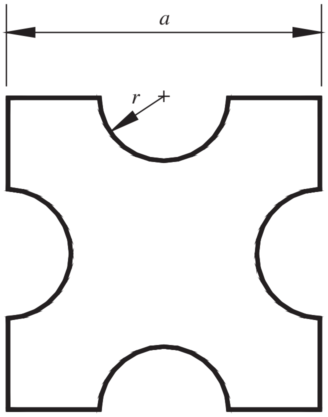

Fig. 8. Geometry of a square plate with semi-circular edge cuts.

Table 6
Linear frequency parameters ($\lambda_L = \omega_L a^2 \sqrt{\rho h/D}$) and period ratios ($T_{NL}/T_L$) of the simply supported square plate with edge cuts ($2r/a = 0.4$, $a = 2$)

Number of points	Order of scheme	λ_L	W_{max}/h					
			0	0.2	0.4	0.6	0.8	1.0
			Fundamental mode					
1020	20	56.485	1.0	0.9852	0.9446	0.8873	0.8225	0.7573
1020	27	56.530	1.0	0.9835	0.9388	0.8766	0.8076	0.7394
1552	20	56.462	1.0	0.9857	0.9463	0.8903	0.8268	0.7625
1552	27	56.461	1.0	0.9849	0.9436	0.8853	0.8197	0.7539
2445	20	56.459	1.0	0.9862	0.9482	0.8938	0.8318	0.7686
2445	27	56.469	1.0	0.9852	0.9446	0.8872	0.8224	0.7572
			Second mode					
1020	20	113.875	1.0	0.9785	0.9217	0.8462	0.7668	0.6917
1020	27	113.997	1.0	0.9779	0.9197	0.8429	0.7624	0.6868
1552	20	113.888	1.0	0.9779	0.9197	0.8428	0.7623	0.6866
1552	27	113.913	1.0	0.9711	0.8980	0.8068	0.7165	0.6358
2445	20	113.896	1.0	0.9800	0.9267	0.8550	0.7784	0.7051
2445	27	113.921	1.0	0.9765	0.9152	0.8352	0.7524	0.6755
			Third mode					
1020	20	134.336	1.0	0.9785	0.9217	0.8462	0.7668	0.6917
1020	27	134.544	1.0	0.9742	0.9079	0.8229	0.7367	0.6579
1552	20	134.324	1.0	0.9780	0.9201	0.8435	0.7632	0.6876
1552	27	134.368	1.0	0.9762	0.9142	0.8335	0.7502	0.6730
2445	20	134.318	1.0	0.9794	0.9247	0.8514	0.7736	0.6996
2445	27	134.375	1.0	0.9767	0.9160	0.8366	0.7542	0.6774

clamped plate) and the two LSFD schemes are adopted to investigate the convergence behaviors of the LSFD solutions. It can be seen from the results that the convergence behaviors of λ_L and T_{NL}/T_L values for both boundary conditions and all three modes are rather stable. The presented mode shapes are also very smooth. For this plate shape, there is no data in the literature for comparison. But the good convergence behaviors of the LSFD solutions and the smoothness of the mode shapes for this complicated plate shape, together with the good results for other previous plate shapes, lend credibility to the correctness and accuracy of the LSFD method for large-amplitude vibration of plates.

Table 7
Linear frequency parameters ($\lambda_L = \omega_L a^2 \sqrt{\rho h/D}$) and period ratios ($T_{\mathrm{NL}}/T_L$) of the clamped square plate with edge cuts ($2r/a = 0.4$, $a = 2$)

Number of points	Order of scheme	λ_L	$W_{\max}/h$					
			0	0.2	0.4	0.6	0.8	1.0
			Fundamental mode					
1020	20	92.765	1.0	0.9937	0.9754	0.9472	0.9117	0.8716
1020	27	92.966	1.0	0.9903	0.9629	0.9221	0.8731	0.8205
1552	20	92.661	1.0	0.9940	0.9766	0.9496	0.9155	0.8768
1552	27	92.625	1.0	0.9928	0.9722	0.9407	0.9014	0.8577
2916	20	92.579	1.0	0.9950	0.9806	0.9579	0.9287	0.8949
2916	27	92.575	1.0	0.9951	0.9807	0.9581	0.9291	0.8955
			Second mode					
1020	20	177.573	1.0	0.9842	0.9413	0.8810	0.8138	0.7468
1020	27	178.081	1.0	0.9855	0.9457	0.8892	0.8252	0.7605
1552	20	177.505	1.0	0.9885	0.9564	0.9094	0.8543	0.7966
1552	27	177.543	1.0	0.9868	0.9501	0.8975	0.8370	0.7750
2916	20	177.356	1.0	0.9906	0.9642	0.9246	0.8768	0.8253
2916	27	177.427	1.0	0.9903	0.9628	0.9220	0.8729	0.8202
			Third mode					
1020	20	219.267	1.0	0.9872	0.9517	0.9006	0.8415	0.7805
1020	27	219.951	1.0	0.9851	0.9443	0.8867	0.8216	0.7562
1552	20	219.141	1.0	0.9888	0.9575	0.9116	0.8574	0.8005
1552	27	219.242	1.0	0.9871	0.9514	0.8999	0.8405	0.7793
2916	20	218.891	1.0	0.9915	0.9672	0.9306	0.8859	0.8371
2916	27	219.005	1.0	0.9898	0.9609	0.9182	0.8672	0.8129

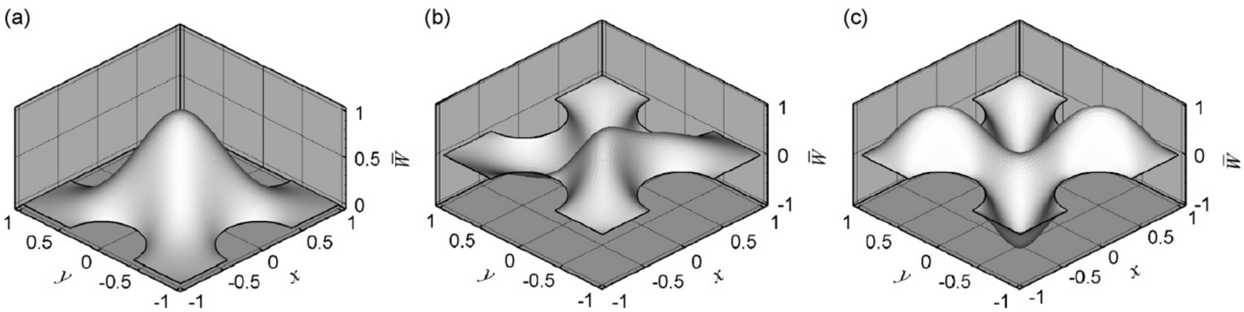

Fig. 9. Free vibration mode shapes of the simply supported square plate with semi-circular edge cuts: (a) first mode, (b) second mode and (c) third mode.

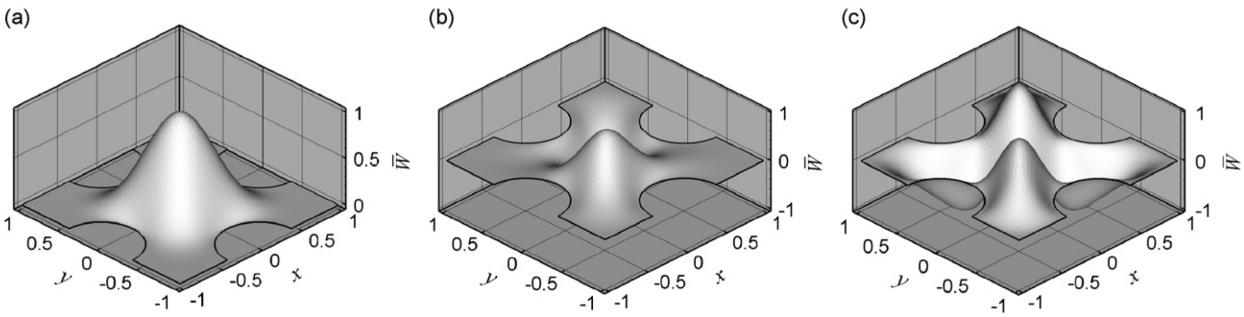

Fig. 10. Free vibration mode shapes of the clamped square plate with semi-circular edge cuts: (a) first mode, (b) second mode and (c) third mode.

7. Conclusions

The mesh-free LSFD method has been used to analyze the large-amplitude vibration of elastic, thin plates with arbitrary shapes and different combinations of boundary conditions. By neglecting the effect of stretching in-plane forces on the mode shapes and the effects of coupling between different vibration modes, the mode shapes of the large-amplitude vibration of plates can be regarded as similar to the mode shapes of their linear small-amplitude vibration counterparts. Therefore, the transverse modal deflection of the plate can be readily solved by using the LSFD method and the classical thin plate theory for plates with small deflections. The longitudinal displacements of plate elements can then be calculated from the coupling relations between the transverse deflection and longitudinal displacements. These relations are given by the equations of motion of the plate elements in x and y directions. Finally, the equation of motion of plate elements in transversal direction is transformed into an ODE of a periodic temporal function, from which the frequencies or periods of the large-amplitude vibration can be solved by using a simple FDM. The effects of large amplitudes on the vibration periods are reflected by the varying values of the ratio T_{NL}/T_L.

As revealed in previous sections, a critical step in the large-amplitude vibration analysis of plates is the solution of the linear governing PDE of small-amplitude vibration of plates. If accurate solutions can be obtained for the linear PDE, then accurate solutions for relevant large-amplitude vibration can also be obtained. As illustrated in this paper, the LSFD method is a powerful tool for tackling this type of problems. There are two basic features that ensure the high accuracy and versatility of the LSFD method. One is the mesh-free property that enables the LSFD method to accommodate problems with arbitrary domain shapes. Another property is the high-order local approximation that enables the method to achieve high accuracy for solutions. Owing to these two features, the LSFD method has been successfully used to furnish highly accurate numerical solutions for both linear small-amplitude and nonlinear large-amplitude vibration analysis of plates with simple and complex domain shapes.

References

[1] S.P. Timoshenko, S. Woinowsky-Krieger, *Theory of Plates and Shells*, second ed., McGraw-Hill, New York, 1959.

[2] A.C. Ugural, *Stresses in Plates and Shells*, second ed, McGraw-Hill, New York, 1999.

[3] A.W. Leissa, *Vibration of Plates*, NASA, 1993.

[4] H.N. Chu, G. Herrmann, Influence of large amplitudes on free flexural vibrations of rectangular elastic plates, *Journal of Applied Mechanics* 23 (1956) 532–540.

[5] N. Yamaki, Influence of large amplitudes on flexural vibrations of elastic plates, *ZAMM* 41 (1961) 501–510.

[6] H.M. Berger, A new approach to the analysis of large deflections of plates, *Journal of Applied Mechanics* 22 (1955) 465–472.

[7] T. Wah, Large amplitude flexural vibration of rectangular plates, *International Journal of Mechanical Sciences* 5 (1963) 425–438.

[8] C. Mei, Finite element displacement method for large amplitude free flexural vibrations of beams and plates, *Computers and Structures* 3 (1973) 163–174.

[9] G.V. Rao, I.S. Raju, K.K. Raju, A finite element formulation for large amplitude flexural vibrations of thin rectangular plates, *Computers and Structures* 6 (1976) 163–167.

[10] G.V. Rao, K.K. Raju, I.S. Raju, Finite element formulation for the large amplitude free vibrations of beams and orthotropic circular plates, *Computers and Structures* 6 (1976) 169–172.

[11] C. Mei, R. Narayanaswami, G.V. Rao, Large amplitude free flexural vibrations of thin plates of arbitrary shapes, *Computers and Structures* 10 (1979) 675–681.

[12] X.X. Wang, J. Qian, M.K. Huang, A boundary integral equation formulation for large amplitude nonlinear vibration of thin elastic plates, *Computer Methods in Applied Mechanics and Engineering* 86 (1991) 73–86.

[13] Y. Shi, C. Mei, A finite element time domain modal formulation for large amplitude free vibrations of beams and plates, *Journal of Sound and Vibration* 193 (1996) 453–464.

[14] L. Kurpa, G. Pilgun, E. Ventsel, Application of the *R*-function method to nonlinear vibrations of thin plates of arbitrary shape, *Journal of Sound and Vibration* 284 (2005) 379–392.

[15] M. Barik, M. Mukhopadhyay, A new stiffened plate element for the analysis of arbitrary plates, *Thin-Walled Structures* 40 (2002) 625–639.

[16] H. Ding, C. Shu, K.S. Yeo, D. Xu, Development of least square-based two-dimensional finite difference schemes and their application to simulate natural convection in a cavity, *Computers and Fluids* 33 (2004) 137–154.

[17] C. Shu, W.X. Wu, H. Ding, C.M. Wang, Free vibration analysis of plates using least-square-based finite difference method, *Computer Methods in Applied Mechanics and Engineering* 196 (2007) 1330–1343.

[18] C.M. Wang, W.X. Wu, C. Shu, T. Utsunomiya, LSFD method for vibration analysis of plates with free edges, *Advances in Steel Structures*, *ICASS'05*, 2005, pp. 1715–1722.
[19] W.X. Wu, C. Shu, C.M. Wang, Computation of modal stress resultants for completely free vibrating plates by LSFD method, *Journal of Sound and Vibration* 297 (2006) 704–726.
[20] C.M. Wang, W.X. Wu, C. Shu, T. Utsunomiya, LSFD method for accurate vibration modes and modal stress-resultants of freely vibrating plates that model VLFS, *Computers and Structures* 84 (2006) 2329–2339.
[21] C. Shu, W.X. Wu, C.M. Wang, Least squares finite difference method for vibration analysis of plates, in: N.E. Shanmugam, C.M. Wang (Eds.), *Analysis and Design of Plated Structures: Dynamics*, vol. 2, Woodhead Publishing Limited, Cambridge, England, 2006 (Chapter 4).
[22] J.S. Chen, C.H. Pan, C.T. Wu, W.K. Liu, Reproducing kernel particle methods for large deformation analysis of non-linear structures, *Computer Methods in Applied Mechanics and Engineering* 139 (1996) 195–227.
[23] Q.S. Li, Y.Q. Huang, Moving least-squares differential quadrature method for free vibration of antisymmetric laminates, *Journal of Engineering Mechanics* 130 (12) (2004) 1447–1457.
[24] K.M. Liew, Y.Q. Huang, J.N. Reddy, Moving least squares differential quadrature method and its application to the analysis of shear deformable plates, *International Journal for Numerical Methods in Engineering* 56 (15) (2003) 2331–2351.
[25] W.K. Liu, S. Jun, S.F. Li, J. Adee, T. Belytschko, Reproducing kernel particle methods for structural dynamics, *International Journal for Numerical Methods in Engineering* 38 (1995) 1655–1679.
[26] L.X. Peng, K.M. Liew, S. Kitipornchai, Buckling and free vibration analyses of stiffened plates using the FSDT mesh-free method, *Journal of Sound and Vibration* 289 (2006) 421–449.